Electroanalysis at Discrete Arrays of Gold Nanowire Electrodes

Karen Dawson, Marine Baudequin, Nicolas Sassiat, Aidan J. Quinn and Alan O'Riordan*

Nanotechnology Group, Tyndall National Institute-University College Cork, Lee Maltings, Dyke Parade, Cork, Ireland.

*Corresponding author: alan.oriordan@tyndall.ie

Abstract:

The development of reliable nanosensors proffers a number of potential advantages in nanoscale analytical science. A hybrid electron beam-photolithography process was used to fabricate robust and reliable electrochemical nanowire array devices, with highly reproducible critical dimensions, 100 ± 6 nm. Nanowire electrode arrays were designed to permit diffusional independence at each nanowire element in an array thereby maximising limiting currents for optimised electrochemical nanosensing. The electrochemical behaviour of discrete nanowire electrode arrays was investigated using cyclic voltammetry in ferrocenemonocarboxylic acid. Single nanowire devices yielded highly reproducible steady-state sigmoidal waveforms, with typical currents of 179 ± 16 pA. Higher steady-state currents were achieved at nanowire arrays, up to ~1.2 nA for arrays consisting of six nanowire elements. At low and intermediate scan rates, sigmoidal waveforms were observed for nanowire arrays indicating very fast mass transport. However, voltammetric behaviour consistent with semi-infinite linear diffusion was observed at higher scan rates confirming the presence of overlapping diffusion profiles between neighbouring nanowires within an array. The

existence of diffusion overlap between neighbouring nanowire elements was further demonstrated by deviation of measured steady-state currents with estimates, becoming more pronounced with increasing numbers on nanowire elements in the array. Finally capacitive charging of the electrodes were explored, and were found to exhibit very low capacitance typically ~ 31 ± 3 nF cm^{-2} per device three orders of magnitude less than that reported for conventional microelectrodes (~20 μF cm^{-2}).

1. Introduction:

The development of reliable ultra-small electrodes offers numerous potential advantages for both electrochemistry and analytical nanoscience. [1-4] Enhanced electrochemical sensitivity arises from improved mass transport of the nanoscale electrodes offering the potential for kinetic measurements of faster electrochemical processes. [5] Other advantages include: shorter response times, lower RC constants, low analyte depletion and greatly reduced sample volumes. [6] Finally, smaller electrodes dimensions should enable nanosensors to be fabricated at high density, at technologically relevant substrates, such as at a silicon chip, thus yielding much higher information-generating capability per device. [7, 8]

In electrochemistry, work at very small (sub-micrometre) electrode sizes at silicon substrates, has mainly been restricted to electrochemically favourable geometries, such as nanodisks, nanopores and short inlaid nanobands. [5, 9-13] However, when employed as discrete electrodes, these structures can have extremely low measurable signals (typically < 100 pA) [8, 14, 15] and require large electrode numbers in array format (> 10 x 10) to realise reasonable measureable currents, i.e. in the nanoAmpere range. [8, 16, 17] To address this challenge, researchers have recently begun to explore high aspect ratio 1-dimensional discrete nanoelectrodes such as nanobands and nanowires. [18-23] This newer class of nanoelectrode benefits from radial

diffusion due to their nanometre scale critical dimension while achieving relatively large currents (nA) due to the long length of the electrode, typically ≥40 m. [9, 20, 22, 23] To date however, few approaches for the fabrication of robust, high-aspect-ratio, discrete nanowire electrodes with reproducible dimensions and repeatable measureable currents have been studied. [18-22]

Recent publications have highlighted the key attributes of 1-dimensional electrodes, demonstrating fast analyte mass transport and steady-state behaviour under standard voltammetric conditions. [18-21, 24] These desirable electrochemical properties were subsequently exploited to determine rates of electron transfer for the model redox mediators yielding, in some cases, rates two orders of magnitude higher than that previously reported. [18, 20, 25] Recently we reported, reported two different approaches for the fabrication of single nanowire electrodes; Nanoskiving and E-beam lithography, respectively. These devices were successfully applied to the very sensitive detection of important biomolecules, such as hydrogen peroxide and glucose. [18, 19] Arrays of nanowires offer the potential for further enhancements in sensitivity, should the wires be sufficiently spaced so as to prevent diffusional overlap. In this work, we fabricate and characterised electrodes based on discrete nanowire arrays for electroanalysis.

We employ electron-beam lithography (EBL) to fabricate gold nanowire arrays strategically designed with sufficient inter-nanowire spacing so as to prevent diffusional overlap occurring at adjacent nanowire elements within an electrodes array. Nanowire and nanowire array devices were structural and functionally characterised using a combination of optical and electron microscopy and two-point electrical measurements. Cyclic voltammetry employing a model redox probe;

FcCOOH, was used to explore mass transport behaviour at the nanowire arrays. In depth analysis of the electrochemical properties of nanowire electrode arrays was undertaken, including comparison with theoretical models. Finally, the variation in capacitive contributions and the consequent effects on signal to noise ratios was investigated.

2. Experimental:

2.1 Nanowire Fabrication:

Nanowire electrodes were fabricated using a hybrid electron beam-photolithography process on four inch thermally oxidised silicon wafer substrates (~300 nm SiO_2), see Fig 1. In this approach, nanowire and alignment marks were written by direct write electron beam lithography (JBX-6000FS, JEOL UK Ltd., optimised parameters: beam voltage 50 kV, beam current 100 pA and beam dose 120 C cm^{-2}) in resist (ZEP 520 Nippon Zeon). Following resist development, (Ti 5 nm/Au 30 nm) layers were blanket deposited by evaporation (Temescal FC-2000 E-beam evaporator) and standard lift-off techniques were used to remove un-patterned areas thus yielding nanowire structures. Using alignment marks written by EBL for alignment and registration, micronscale interconnection tracks were then easily overlaid onto nanowire termini using photolithography, metal deposition (Ti 10 nm/Au 200 nm) and lift-off techniques. Each chip contained six different individually addressable nanowire arrays, ranging from single nanowires up to six nanowire electrodes per array. A ~1 m thick layer of photoresist (Shipley S1813) was then spin coated onto the wafer surface and patterned using photolithography to open a window (~40 m x 50 m) in the photoresist directly above the nanowire arrays. This process was optimised such that the interconnection tracks remained covered by the insulating

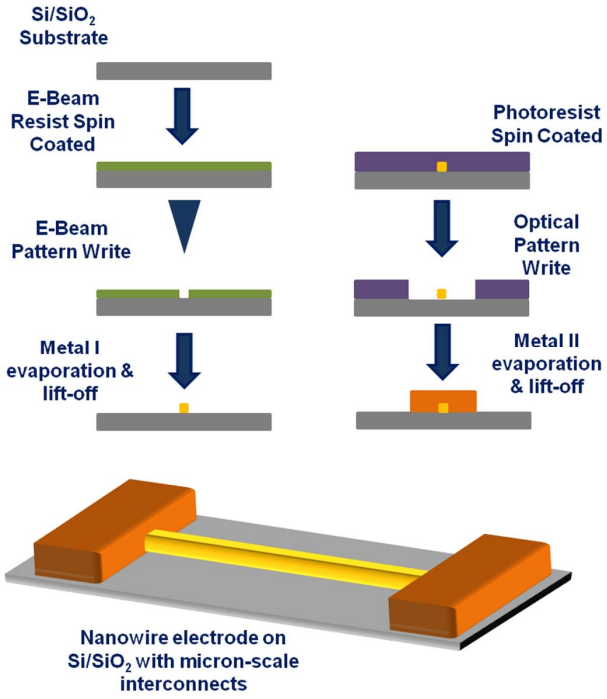

Figure 1: Schematic of nanowire electrode fabrication by hybrid EBL-photolithography.

photoresist layer thereby permitting direct contact exclusively between a nanowire array and the external electrolyte solution. Finally, to complete device packaging,chips were assembled onto specifically designed printed circuit boards (PCB), electrically contacted using wedge wire bonding (25 µm gold wires) and the bond wires protected using epoxy. Control devices, without a nanowire present, were fabricated in an identical manner.

2.2 Nanowire Characterisation:

Structural characterisation of nanowires was undertaken using scanning electron microscopy. SEM was acquired using a field emission SEM (JSM-7500F, JEOL UK Ltd.) operating at beam voltages between 5 and 10 kV. Images were captured employing both the standard secondary electron detector (SE) and a back scattered electron detector (BSE). Two-point electrical measurements were performed using a probe station (Model 6200, Micromanipulator Probe Station) in combination with a

source meter (Keithly 2400) programmed using LabVIEW™. In these current-voltage (*I-V)* measurements, the source electrode was grounded, a bias sweep up to ± 10 mV was applied to the drain electrode, and the current through the nanowire was measured.

2.3 Electrochemical Analysis:

All electrochemical studies were performed using a CHI660a Electrochemical Analyser and Faraday Cage & Picoamp Booster CHI1200b (CH Instruments). A three-electrode cell was adopted, employing a nanowire electrode array as a working electrode, with platinum coil (BAS Inc.) as a counter electrode and a saturated Ag/AgCl reference electrode (CH Instruments). The PCB-mounted nanowire electrodes were immersed in electrolyte, and a direct electrical connection made to the potentiostat using an edge connector to the probe pin-outs of the PCB. Unless otherwise stated all chemicals were obtained from Sigma Aldrich and used as received. Cyclic voltammograms were recorded at nanowire electrodes in sulphuric acid (H_2SO_4, 0.1 M). Electrochemical studies on FcCOOH (1 mM) (Alfa Aesar) were carried out in 10 mM phosphate buffered saline, (PBS) solutions, at pH 7.4. Cyclic voltammetry measurements were carried out in the potential range of 0.0 V to 0.6 V at a variety of scan rates (5 - 2000 mVs^{-1}). All solutions were prepared with deionised water (resistivity 18.2 MΩ cm, Elga Pure Lab Ultra) and deaereated with N_2 gas prior to electroanalysis.

3. Results and Discussion:

3.1 Nanowire Structural Characterisation:

Individually addressable gold nanowire array electrodes were fabricated using a hybrid EBL and photolithography process at silicon wafer substrates bearing a 300

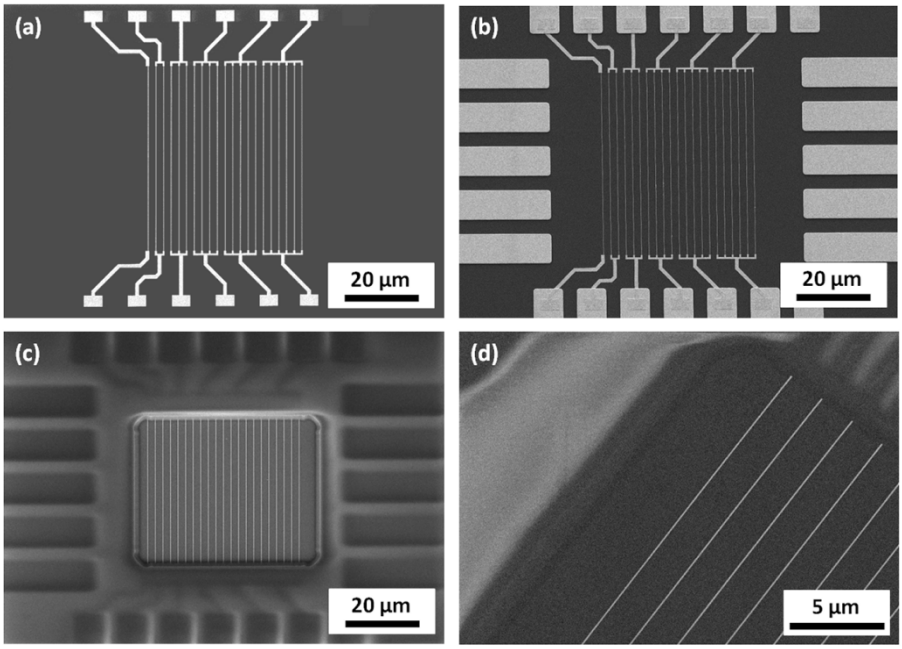

Fig. 2: SEM structural characterization of nanowire electrode arrays. (a) Image of nanowire arrays fabricated by EBL on Si/SiO_2, prior to interconnection deposition. (b) SEM micrograph of nanowire arrays with overlaid interconnection tracks. (c) Fully passivated interconnection tracks with a window opened in the passivation layer above the nanowire electrode arrays. (d) Micrograph in composition mode of nanowire arrays following selective removal of the photoresist passivation. A clear signal from the high atomic mass gold nanostructures is evident compared to the silicon oxide substrate and surrounding photoresist.

nm layer of thermally grown silicon dioxide see the Experimental. Prior to proceeding to subsequent fabrication steps, wafer-scale SEM inspection was first undertaken following nanowire deposition to ensure that nanowire structures were correctly resolved and undamaged; see Fig 2(a). Metal interconnection tracks were then deposited by photolithography, metal deposition and lift-off techniques using the e-beam written alignment marks for registration. SEM microscopy was employed to confirm that the tracks were overlaid correctly onto the microscale termini of nanowires. Excellent alignment of both the EBL and optical patterned metal layers was routinely achieved; see Fig 2(b). High resolution SEM microscopy was also employed to undertake statistical analysis of nanowire critical dimensions yielding a typical electrode width of 100 ± 6 nm, (n= 60).

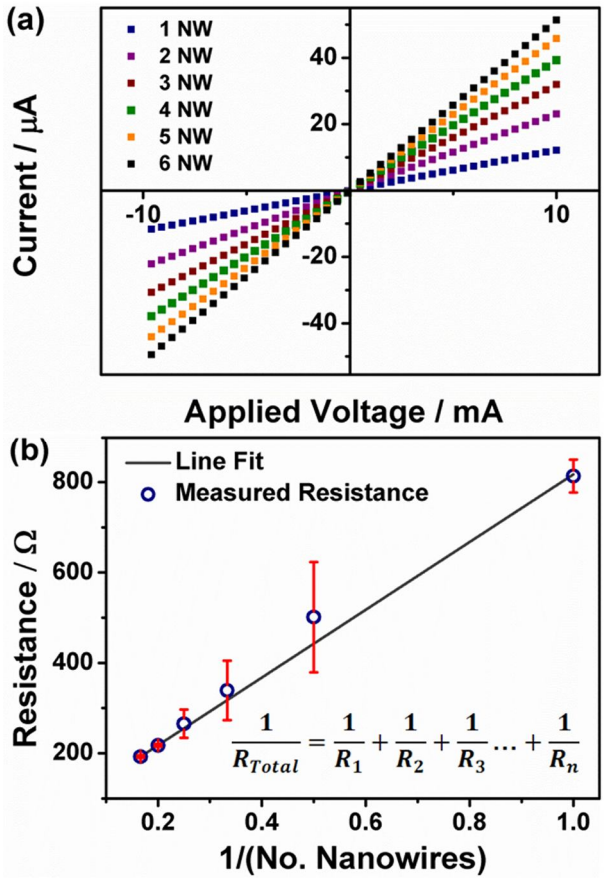

Fig 3: (a) Typical Ohmic responses observed for two point current voltage measurements obtained for nanowire arrays with increasing number of nanowire elements. (b) Plot of total resistance versus inverse number of nanowires present in the array. Inset: Equation for total device resistance where there are resistors positioned in parallel.

To allow direct interaction exclusively between a nanowire and electrolytic solution, photolithography was employed to selectively remove a window (40 x 50 μm), in a photoresist passivation layer, directly above the nanowire array, see Fig 2(c). An enhanced contrast between the conductive gold nanowires and the insulating silicon oxide substrate can be observed in Fig 2(d). A contrast is also observed in this micrograph between the nanowires exposed by passivation opening and where the nanowire termini and the interconnections which are insulated by the photoresist overlayer. This indicates that there is little or no residual photoresist remaining over

the nanowire electrodes. Openings were also made in the photoresist overlayer above the contact pads to allow electrical connections to be formed by wedge wire bonding.

3.2 Nanowire Electrical Characterisation:

Electrical characterisation of nanowire arrays was performed using standard two point *I-V* measurements in air. This was undertaken as a quality control check to ensure that all nanowire electrodes were fully functional prior to electroanalysis. For nanowire devices that were fully functional Ohmic responses were observed. Devices which displayed non-Ohmic behaviour or resistances indicative of a damaged or defective electrodes were discarded and not used for further analysis. An increase in the measured current was observed as the number of the nanowires in an array increased; see Fig 3(a) consistent with an increase in number of conductive pathways. [26] By plotting array resistance versus the inverse number of nanowires (parallel resistors) in the array, see Fig 3(b) and performing regression analysis, the slope of the line yielded an approximate value for the resistance of a nanowire 749 ± 32 Ω, while the intercept yielded a value of 82 ± 18, which is an approximate value for system resistance, i.e., contact resistance, interconnection tracks, probes and leads. Assuming, the resistances associated with interconnection tracks, probes and leads are minimal (1-2 Ω), the contact resistance of the nanowires may be estimated as~80 Ω. This is very low for nanowire devices. [27] Control electrical measurements were also undertaken in the absence of nanowires, yielding very low currents and high resistances (~10 GΩ), typical of an open circuit. This confirmed that the observed Ohmic behaviour of the nanowire electrodes was exclusively due to the nanowire electrodes and associated on-chip metallisation interconnections with no contribution from the underlying silicon substrate.

3.3 Electrochemical Characterisation of Single Nanowires:

Electroanalyses were performed using a potentiostat with a Faraday cage and Picoamp Booster. A standard three-electrode cell setup was adopted with single nanowire and nanowire arrays employed as the working electrode, versus Ag/AgCl (saturated KCl) reference with a Pt coil as a counter electrode. Prior to the electroanalytical investigations, nanowire electrodes were cleaned by potentiodynamic cycling in 0.1 M sulphuric acid for several cycles until a stable reproducible voltammogram was obtained. The resultant voltammograms exhibited gold oxide formation (~1.4 V) and reduction (0.9 V) peaks, characteristic of a gold electrode, see Fig 4(a). [28, 29] No other peaks were observed confirming that at the SiO_2 substrate and the titanium adhesion layer where electrochemically inert at the applied voltage range, see inset Fig 4(a). Typically, the magnitudes of the gold reduction peaks were observed to be between 0.1 and 0.4 nA (varying for from 1-6 nanowire elements). We attribute these low currents exclusively to the electrochemical reduction of gold oxide formed on the surface of a nanowire electrode, strongly suggesting that the photoresist passivation layer successfully insulated the interconnection tracks from the electrolyte.

To explore the electrochemical properties of these nanowire array devices, we selected FcCOOH as the model analyte chosen for its simple redox chemistry and low overpotentials. [8, 30] Fig 4(b) (navy line) depicts a typical cyclic voltammogram (CV) acquired using a gold single nanowire device in deaereated 1 mM FcCOOH in 10 mM PBS, pH 7.4 and 20 ºC. The observed response for all single nanowires was sigmoidal and steady-state, typical of a nanoelectrode undergoing single electron oxidation. Very low hysteresis between the forward and reverse scan was observed, indicating very low capacitive effects (discussed further below). The steady-state

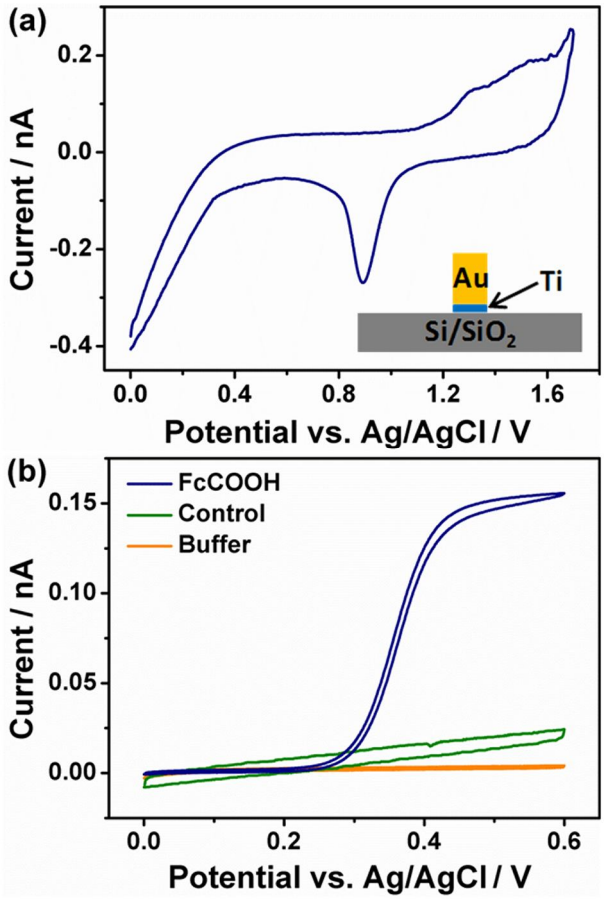

Fig 4: (a) A typical cyclic voltammogram obtained for a single gold nanowire electrode in 0.1 M H_2SO_4 (N_2 sat) from 0.0 V to 1.7 V vs. Ag/AgCl at 100 mV s^{-1}. Inset: Schematic of the cross-section of the nanowire electrode. (b) Typical CV measured at a single nanowire electrode in the presence (navy line) and absence (orange line) of 1 mM FcCOOH in 10 mM PBS, pH 7.4, N_2 Sat at 5 mV s^{-1}. Data for a control device (contact electrodes only, no nanowire 1 mM FcCOOH) are also shown (green line).

behaviour arises from rapid mass transport of the analyte to the electrode borne out by radial diffusion to the very small critical dimensions of the electrode. This facilitates rapid replenishment of the reacted analyte at the electrode surface. The dominance of radial diffusion observed at nanoelectrodes is critical to their behaviour. However, electrodes such as nanowires that have a high aspect ratio, not only benefit from the radial diffusion owing to the nanoscale critical dimension, but also a very high electroactive area arising from their long length ≈40 m. This dual advantage permits nanowire electrodes to achieve much higher measureable currents, typically 2 orders

of magnitude, than nanodisk or nanopore electrodes with similar critical dimensions. [31]

EBL lithography has been shown to be a highly reproducible technique for the fabrication of nanowire electrodes. [18-20] In this regard, we undertook electroanalysis at several nanowire electrode arrays consisting of one electrode element to assess the reproducibility of the electrochemical responses. In all cases, sigmoidal voltammograms were observed with an average steady-state current of 179 ± 16 pA on 6 different chips (n=30), correlating to a standard deviation of ~9 %. This correlates well with the observed variations in nanowire dimension in *Section 3.1* and is good agreement with steady-state currents previously observed for single nanowire electrodes of similar dimensions previously reported. [19] The variation in measured signal at single nanowires may be accounted for by differences in the exact nanowire electrode surface area arising from gold clustering during the thermal evaporation process and rough nanowire edges created during the metal evaporation and lift-off processes. [18-20]

Voltammetry undertaken in the absence of FcCOOH, i.e., in 10 mM PBS yielded no Faradic current, see Fig 4(b) orange line. Under these conditions very low background currents were recorded ~ 1 pA, ideal for sensor applications. CV experiments were also undertaken employing control devices (no nanowires present) in 1 mM FcCOOH in 10 mM PBS electrolyte. As can be seen in Fig 4 (green line), these control devices did not display Faradic current, indicating that there was no oxidation of the analyte at the silicon dioxide surface or the insulated interconnection tracks. The slight increase in measured current and hysteresis may be due to

increased charging arising from the solution being in-completely deaereated. Typical charging currents measured from control devices at low scan rates ~ 5-10 pA.

Having established that the electrochemical responses observed in Fig 4(b) (navy line) were exclusively attributed to the nanowire electrodes, we proceeded to benchmark it against a relevant theoretical model. In this regard, we estimated the limiting current at an inlaid nanoband as approximated by equation (1) below, derived from the hemicylinder limiting current equation, in which r is defined as $w/4$: [3, 31, 32]

$$i_L = \frac{2\pi F l D_O C^*}{\ln(64 D_O t / w^2)} \quad (1)$$

where n is the number of electrons transferred, F is Faraday's constant, C^* is the bulk concentration of the mediating species, D_O is the diffusion coefficient (5.4×10^{-6} cm^2 s^{-1}), [30] l is the length of the band electrode and t is the time (equal to RT/Fv, where R is the gas constant, T is temperature, v is the scan rate) and w is electrode width. Although this equation does not take into consideration the nanowire height, it has been shown previously to provide a good approximation for expected limiting current of nanowire electrodes. [20] Inserting values of width = 100 nm and electrode length = 40 m into equation (*1*), limiting currents were estimated to be ~810 pA at a scan rate of 5 mV s^{-1}, which is significantly higher than that average measured for single nanowire electrodes ~179 pA. Similar deviation from expected limiting currents was observed by Gracias *et al* [22], at single nanowires with critical dimensions of ~30 nm. However, the high reproducibility in the experimentally obtained current values (~ 9% variation), measured across a number of chips strongly suggests that nanowire surfaces were pristine, this is further supported by the SEM data presented in Fig 2(d).

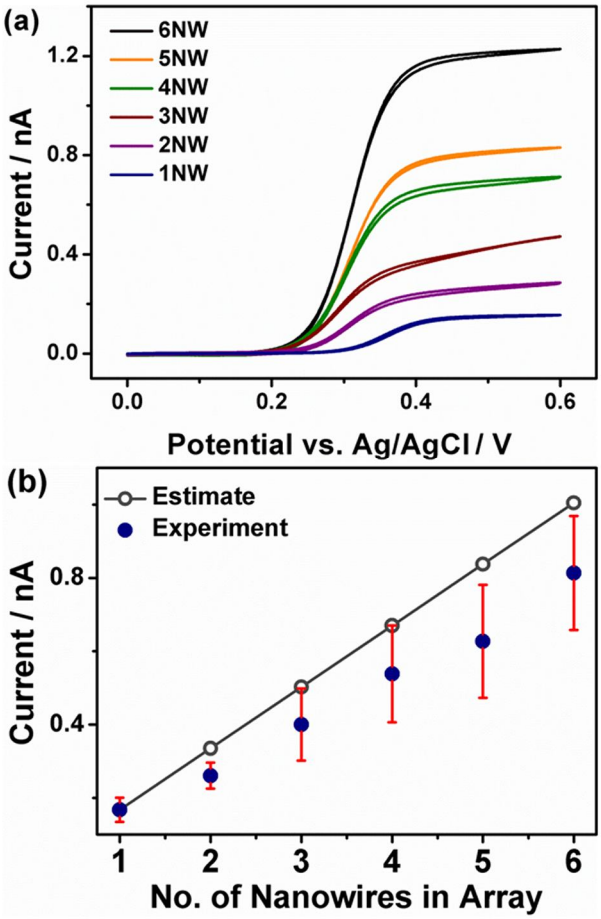

Fig 5: (a) Voltammetric characterization for nanowire electrode arrays with increasing number of nanowire elements in 1 mM FcCOOH in 10 mM PBS, pH 7.4, N_2 Sat, at 5 mV s^{-1}. (b) Increase in the average steady state current values (n=30 per array type) recorded at 5 mV s^{-1} for increasing numbers of nanowires in arrays (navy data point). Expected current values for these nanowire arrays extrapolated from the single nanowire current average are included in grey.

Work is now on-going using different height nanowires to explore this deviation further.

3.4 Analysis of Electrochemical Behaviour at Nanowire Arrays:

As previously mentioned, nanoelectrode arrays have tremendous potential in areas of electrochemical applications; particularly in the field of nanosensors. Provided each individual electrode in the array is diffusionally independent, they have the ability to maximise the measureable signal whilst maintaining the advantages of the nanoscale. In order to ensure this behaviour across a nanoelectrode array, the electrodes must be

sufficiently separated such that neighbouring radial diffusion profiles do not overlap with each other, resulting in undesirable quasi-planar type diffusion. Successful design of the nanowire arrays to achieve this desired diffusional independence requires knowledge of the thickness of the radial diffusion profile of a single nanowire. To achieve this, the thickness of the Nernstian diffusion layer at a nanoband electrode was estimated by the following expression where w = 4*r*: [3]

$$\delta = w\ln 64(D_O t/w^2) \qquad (2)$$

D_O is the diffusion coefficient (5.4 x 10^{-6} cm^2 s^{-1}), and *t* is the time. This equation infers the thickness of a diffusion profile; from the electrode surface, where *C=0,* to bulk solution; *C*=1*. To ensure diffusion profiles did not overlap, electrodes would be required to be spaced >2δ. By employing Equation (2), we estimated that under steady-state conditions (120s for a scan rate of 5 mV s^{-1}), subsequent to an oxidative potential step the thickness of the diffusion layer would be on the order of ~250 nm (1δ equivalent to ~10*r)*. Therefore, to be diffusionally independent, nanowires should require a minimum interelectrode separation of ~500 nm (2δ or ~20*r*). However, at the nanoscale, where diffusion profiles have similar dimensions to the diffuse double layer and electrodes typically have non-ideal electrode geometries (such as nanowires) the required inter-electrode spacing may have to be higher to ensure diffusion independence. This has recently been shown to be the case for recessed nanopore electrodes where the spacing should be thirty times the diameter (60*r*) [16]. To this end we designed our inter-electrode spacing to be 1.5 μm, i.e. 60 times w/4 (*r*).

We undertook to experimentally confirm this behaviour by performing cyclic voltammetry in FcCOOH in 10 mM PBS at arrays of nanowire electrodes, ranging

from one up to six nanowire elements per array, with an interelectrode distance of 1.5 m. Fig. 5(a) shows typical voltammograms obtained for different nanowire arrays at 5 mV s^{-1}, displaying sigmoidal waveforms. This suggests that either: (i) nanowires within an electrode array experience fast mass transport and are diffusionally independent, or (ii) nanowire electrodes are not diffusionally independent, but the overall electrode array behaves as an ultramicroelectrode which would also exhibit sigmoidal voltammograms and steady-state currents. However under the latter conditions the currents yielded would be expected to be reduced in magnitude from those attainable at nanowire arrays that had independent diffusion profiles. [3, 16, 33]

To examine the magnitude of limiting current at each array, ideal arrays would behave as a collection of individual electrodes, i.e.; the magnitude of limiting current should be an integer multiple of a single electrode limiting current with respect to the amount of electrodes present in the array, (i.e. i_L for a 6 nanowire array should equal 6 times i_L for 1 nanowire array). Voltammetry of each array type was undertaken using multiple devices in 1 mM FcCOOH. The average measured steady-state signal at each type of nanowire arrays is shown in Fig. 5(b) (navy circles). The error bars represent ± 1 standard deviation from the average results obtained for each devices type (n=30). In order to provide an estimated current for each array, integer multiples of the average measured current for a single nanowire were calculated for the corresponding number of nanowires in each array and plotted, see Fig 5(b) (grey circles). While the measured responses were found to have a strong linear correlation ($R^2 = 0.998$) as the number of nanowires increased, it was observed the recorded steady-state current values deviated from the expected current trend. This marked deviation between the estimated and experimental values, strongly suggest that overlap between neighbouring radial diffusion profiles exist at each nanowire element within an array.

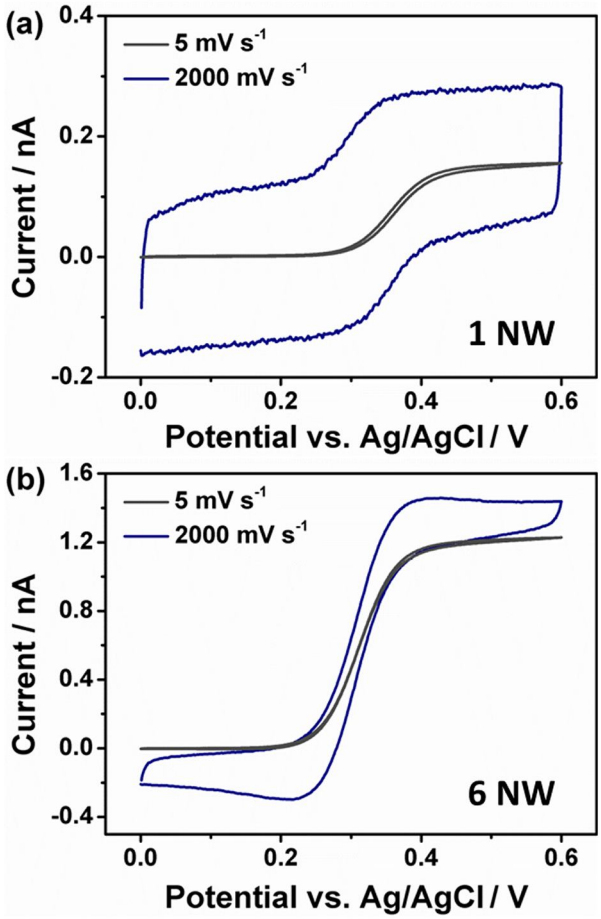

Fig 6: Cyclic voltammograms obtained in 1 mM FcCOOH in 10 mM PBS, pH 7.4, N_2 sat at 5 mVs^{-1} and 2000 mV s^{-1} (a) at a single nanowire electrode and (b) at a six nanowire array.

These overlapping diffusion profiles resulted in a reduction in the measureable electrochemical response i.e., an analyte molecule can only diffuse to one or other of the neighbouring nanowires and not to both, see Fig 6(b). This would imply that in contrast to the estimation based on equation (2), the electrodes were insufficiently separated to permit diffusional independence to each nanowire in the array. Despite this diffusional overlap, at low scan rates (<100 mV s^{-1}) sigmoidal voltammograms were observed for all arrays with all achieving steady-state currents see Fig 5(a). This is in agreement with previous reports using nanoscale electrode arrays [8, 16, 30] and arises from partial and complete diffusional overlap, where the nanowire array it behaves as ultra-microelectrode of the same size of the total array, i.e., the width of a

six nanowire array is 6.6 μm. Such ultramicroelectrodes also experience enhanced mass transport and exhibit sigmoidal behaviour and steady-state currents. [3]

To further confirm that this deviation from expected independent electrochemical behaviour was due to diffusional overlap and not a fabrication related effect, we investigated the effect of variation in scan rate on the measured response at arrays with increasing numbers of nanowires. A broad range of scan rates were examined from very low speeds 5 mV s^{-1} up to quite high rates 2000 mV s^{-1}. At single nanowire electrodes the behaviour observed at both slow and fast scan rates changes very little, see Fig 6(a). Both voltammograms were steady-state and had a sigmoidal shape, while the minimal increases in measured signal can be attributed to capacitive effects. This would indicate that radial profiles existed at all scan rates at single nanowire electrode elements. However, when the same characterisation was undertaken at larger arrays; such as those containing 6 nanowires, a marked difference in the voltammetric behaviour was noted; see Fig 6(b). At higher scan rates and with increasing number of nanowire elements within an array, the voltammograms were noted to have distinctive oxidation and reduction peak, rather than the sigmoidal shape observed at lower scan rates (<100 mV s^{-1}). This behaviour is more consistent with much larger electrodes that experience semi-infinite linear diffusion than nanoelectrode arrays with independent radial diffusion profiles. From this, we could conclude that the lower than expected currents measured for nanowire arrays at low scan rates (5 mV s^{-1}) was due to diffusional overlap. While the long measurement times enabled sufficient analyte replenishment to permit steady-state like conditions to occur. At high scan rates, where the measurement time was dramatically reduced, the overlapping diffusion profiles were revealed. [16] To this end, we conclude that Equation (2) not be sufficient to provide all the relevant information required to

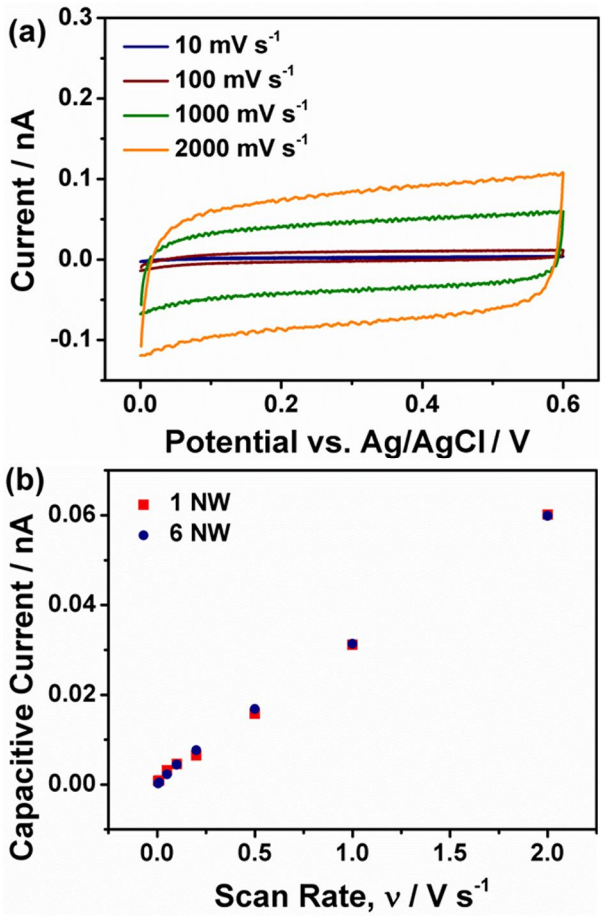

Fig 7: (a) Voltammetric response of a single nanowire in the presence of electrolyte only, 10 mM PBS, at a range of scan rates from 10-2000 mV s^{-1}. (b) Linear dependence of capacitive current on scan rate observed for a single nanowire electrode array (red squares) and a six nanowire electrode array (navy circles) in 10 mM PBS, N_2 sat, pH 7.4.

design nanowire electrode arrays that have independent diffusion profiles to each nanowire electrode element. Work is now on going to model using finite element analysis to further explore the diffusional overlap and optimise nanowire array design.

3.5 Characterisation of Capacitive Contributions:

As mentioned in the previous section, nanowire electrodes were observed to have increased changing currents at higher scan rates, due to the charging of the interfacial double layer at an electrode. To analyse these capacitive contributions at both single nanowires and nanowire arrays, we undertook cyclic voltammetry in deaereated 10 mM PBS buffer in the absence of a redox active species. [8, 31, 34] The magnitude

of charging currents or capacitive currents, i_C, measured under voltammetric conditions is linearly proportional on the scan rate of the voltage sweep. [31, 34] The interfacial capacitance C, may be calculated from the slope of this linear relationship ($m=2AC$), where A is electrode surface area. In this regard, we recorded voltammograms across a broad range of scan rates, 5 - 2000 mV s^{-1} for nanowire electrode arrays ranging from one to six nanowire elements. Fig 7(a) depicts a typical series of voltammograms measured for a single nanowire electrode in 10 mM PBS for a range of scan rates. Under these conditions, no Faradic current was observed at single nanowire electrodes. Similarly, no Faradic currents were observed for nanowire arrays consisting of more than one nanowire element (data not shown). The magnitude of these capacitive (non-Faradic) currents would be expected to vary with electrode area; however voltammograms at nanowire electrode arrays displayed only minimal variations in the magnitude of measured current at equivalent scan rates regardless of the number of nanowires present. This resulted in comparable values of charging current at all scan rates, across different electrode arrays, as can be seen in Fig 7(b) where the average capacitive currents (n=30) for both a single nanowire array and six nanowire arrays are displayed (R^2 =0.999, and 0.998, respectively). This strongly suggests that the measured capacitance may not be solely due to the double layer charging at the nanowire electrodes but also have a dominant contribution from elsewhere. Previous reports on the electrochemical behaviour of nanopore electrode arrays have found similar behaviour also. In these works, it was found that the underlying metallisation dominated to the overall capacitance, such that the creation of extra nanopore electrodes did not affect the measured capacitance. [8, 20, 35] We also found this to be true for the nanowire electrode arrays, whereby increasing the

number of nanowires present in the array did not affect the measured capacitive response.

The values for calculated capacitance were normalised to the area of the nanowire electrode arrays and the metal interconnection tracks. Capacitance values, *C*, were found to be within the range of 30-32 nF cm^{-2} for all nanowire arrays. These values almost a thousand times lower than the capacitance values typically accepted for conventional electrodes; C ≈ 20 F cm^{-2}. [36] This improvement in the capacitive behaviour achieved at nanowire electrodes is due to the nanoscale critical dimensions of the electrode, at which the thickness of the analyte diffusion profiles and the electrolyte double layer are comparable, resulting in reducing charging due to much faster mass transport and reduced solution resistance. [5, 8, 35] This in turn greatly improves the signal-to-noise (S/N) ratios achievable at nanoelectrodes when compared to conventional electrodes.

4. Conclusions:

We have demonstrated a robust and reliable method for the fabrication of electrochemical devices employing arrays of nanowire electrodes. Nanowire arrays, with highly reproducible critical dimensions, were fabricated using a hybrid EBL-photolithography process on silicon substrates and were designed to be diffusionally independent to produce maximised limiting currents for optimised nanosensor development. These devices exhibited Ohmic behaviour with low contact resistances. Electrochemical measurements yielded highly reproducible signals at both single nanowire electrodes and nanowire arrays (~ 9% standard deviation for single nanowire arrays). Voltammetry in FcCOOH at low and intermediate (<100 mV s-1) scan rates was observed to be steady-state and producing sigmoidal voltammograms

with high currents (0.2 -1.2 nA; 1 to 6 nanowire arrays respectively) suggesting that independent diffusion profiles existed at each nanowire present in the arrays. However, comparison of the average steady-state values with the expected values revealed lower than anticipated values for increasing nanowire arrays indicating that nanowire electrodes were not sufficiently separated. High scan rate analysis was undertaken to elucidate the true nature of the observed voltammetric behaviour. Larger arrays of nanowires were found to display voltammetric behaviour more consistent with complete overlap of neighbouring diffusion profiles indicating that an inter-electrode spacing of 1.5 μm were insufficient to maintain independent radial diffusion profiles at these nanoelectrode arrays. Nanowire electrode devices were also found to exhibit very low capacitance typically; ~ 31 ± 3 nF cm-2 per device which is three orders of magnitude less than that expected for microelectrodes (~20 μF cm-2). Work is now on going to optimise the design of nanowire electrode arrays to ensure independent diffusion to electrode in the array and to use the diffusion domain approach to give further insight into the electrochemical behaviour of nanowire arrays.

Acknowledgements:

This work was supported by Science Foundation Ireland under the Research Frontiers Programme (SFI/09/RFP/CAP2455), by the European Commission under the FP7 Security Project CommonSense (261809) and the Irish Higher Education Authority PRTLI programs (Cycle 3 “Nanoscience” and Cycle 4 “INSPIRE”).

References:

[1] R.J. Forster, Chemical Society Reviews, 23 (1994) 289.

[2] A.M. Bond, D. Luscombe, K.B. Oldham, C.G. Zoski, Journal of Electroanalytical Chemistry, 249 (1988) 1.

[3] R.M. Wightman, D.O. Wipf, Electroanalytical Chemistry, 15 (1989) 267.

[4] C.G. Zoski, M.V. Mirkin, Analytical Chemistry, 74 (2002) 1986.

[5] D.W.M. Arrigan, Analyst, 129 (2004) 1157.

[6] A. Lopez-Alemany, J.M. Gonzalez-Meijome, J.B. Almeida, M.A. Parafita, M.F. Refojo, Cornea, 25 (2006) 214.

[7] L. Rassaei, P.S. Singh, S.G. Lemay, Analytical Chemistry, 83 (2011) 3974.

[8] Y.H. Lanyon, G. De Marzi, Y.E. Watson, A.J. Quinn, J.P. Gleeson, G. Redmond, D.W.M. Arrigan, Analytical Chemistry, 79 (2007) 3048.

[9] J.P. Guerrette, S.J. Percival, B. Zhang, Langmuir, 27 (2011) 12218.

[10] B.B. Katemann, T. Schuhmann, Electroanalysis, 14 (2002) 22.

[11] P. Ugo, L.M. Moretto, F. Vezza, Chemphyschem, 3 (2002) 917.

[12] C.J. Slevin, N.J. Gray, J.V. Macpherson, M.A. Webb, P.R. Unwin, Electrochemistry Communications, 1 (1999) 282.

[13] J.J. Watkins, H.S. White, Journal of Electroanalytical Chemistry, 582 (2005) 57.

[14] C.T. Mallon, C. Zuliani, T.E. Keyes, R.J. Forster, Chemical Communications, 46 (2010) 7109.

[15] J.J. Watkins, J.Y. Chen, H.S. White, H.D. Abruna, E. Maisonhaute, C. Amatore, Analytical Chemistry, 75 (2003) 3962.

[16] N. Godino, X. Borrise, F.X. Munoz, F.J. del Campo, R.G. Compton, Journal of Physical Chemistry C, 113 (2009) 11119.

[17] L.M. Moretto, M. Tormen, M. De Leo, A. Carpentiero, P. Ugo, Nanotechnology, 22 (2011).

[18] K. Dawson, J. Strutwolf, K.P. Rodgers, G. Herzog, D.W.M. Arrigan, A.J. Quinn, A. O'Riordan, Analytical Chemistry, 83 (2011) 5535.

[19] K. Dawson, M. Baudequin, A. O'Riordan, Analyst, 136 (2011) 4507.

[20] K. Dawson, A. Wahl, R. Murphy, A. O'Riordan, The Journal of Physical Chemistry C, 116 (2012) 14665.

[21] E.J. Menke, M.A. Thompson, C. Xiang, L.C. Yang, R.M. Penner, Nat. Mater., 5 (2006) 914.

[22] P. Tyagi, D. Postetter, D.L. Saragnese, C.L. Randall, M.A. Mirski, D.H. Gracias, Analytical Chemistry, 81 (2009) 9979.

[23] S.L. Caston, R.L. McCarley, Journal of Electroanalytical Chemistry, 529 (2002) 124.

[24] C. Xiang, A.G. Guell, M.A. Brown, J.Y. Kim, J.C. Hemminger, R.M. Penner, Nano Lett., 8 (2008) 3017.

[25] I. Heller, J. Kong, H.A. Heering, K.A. Williams, S.G. Lemay, C. Dekker, Nano Lett., 5 (2005) 137.

[26] E. Hughes, Hughes Electrical Technology, 6th ed., Longman Scientific & Technical, Glasgow, 1987.

[27] G.D. Marzi, D. Iacopino, A.J. Quinn, G. Redmond, Journal of Applied Physics, 96 (2004) 3458.

[28] L.D. Burke, P.F. Nugent, Gold Bull., 31 (1998) 39.

[29] S. Trasatti, O.A. Petrii, Pure and Applied Chemistry, 63 (1991) 711.

[30] Y.H. Lanyon, D.W.M. Arrigan, Sensors and Actuators B-Chemical, 121 (2007) 341.

[31] A.J. Bard, Faulkner, L.R.,, Electrochemical Methods, Fundamentals & Applications, Second ed., Wiley & Sons.,, New York, 2001.

[32] A. Szabo, D.K. Cope, D.E. Tallman, P.M. Kovach, R.M. Wightman, Journal of Electroanalytical Chemistry, 217 (1987) 417.

[33] S.J. Hood, D.K. Kampouris, R.O. Kadara, N. Jenkinson, F.J. del Campo, F.X. Munoz, C.E. Banks, Analyst, 134 (2009) 2301.

[34] C. Zuliani, D.A. Walsh, T.E. Keyes, R.J. Forster, Analytical Chemistry, 82 (2010) 7135.

[35] J.J. Watkins, H.S. White, Langmuir, 20 (2004) 5474.

[36] C.G. Zoski, Handbook of Electrochemistry, 1st Edition ed., Elsevier, Oxford, 2007.